Development and characterisation of thermally stable supported V-W-TiO_2 catalysts for mobile NH_3-SCR applications

Andrew M. Beale[a,b,c*], Ines Lezcano-Gonzalez [a,b], Teuvo Maunula[d], Robert G. Palgrave[a]

[a]Department of Chemistry, University College London, 21 Gordon Street, WC1H 0AJ, London, UK

[b]UK Catalysis Hub, Rutherford Appleton Laboratory, Research Complex at Harwell, Harwell, Didcot, OX11 0FA, UK

[c]Finden Ltd. Clifton Hampden, Oxfordshire, OX14 3EE, UK

[d]Dinex Ecocat Oy, DET Finland, Catalyst development, Typpitie 1, FI-90620 Oulu, Finland.

*Author to whom correspondence should be addressed: Andrew.Beale@ucl.ac.uk

1. Abstract

Vanadium-based catalysts supported on a mixture of tungsten and titanium oxide (V_2O_5/WO_3-TiO_2) are known to be highly active for ammonia selective catalytic reduction (NH_3-SCR) of NOx species for heavy duty mobile applications. However they are also known to be sensitive to high temperatures which leads to both sintering of the Anatase TiO_2 support and a first order phase transition to Rutile at temperatures > 600 °C. Here we report our attempts to use SiO_2 to stabilise the TiO_2 Anatase phase and to compare its catalytic activity with that of a non-stabilised V_2O_5/WO_3-TiO_2 catalyst after thermal aging up to 800 °C. Detailed characterisation using spectroscopic (Raman, UV-Vis, XANES), scattering and techniques providing information on the catalytic surface (BET, NH_3 adsorption) have also been performed in order to understand the impact of high temperatures on component speciation and the catalytic interface. Results show that non-stabilised V_2O_5/WO_3-TiO_2 catalysts are initially stable after thermal aging at 600 °C but on heating above this temperature a marked drop in catalytic activity is observed as a result of sintering and transformation of Anatase into Rutile TiO_2 and phase segregation of initially highly dispersed WO_3 and polymeric V_2O_5 into monoclinic WO_3 and V_2O_3 crystallites. Similar behaviour was

observed for the 4-5 wt. % of SiO_2-stablised sample after ageing above 700°C, therefore importantly it is offset of thermal stability by some ~ 100 °C.

2. Introduction

Low loaded (~ 2 %) V containing catalysts such as V/TiO_2 are well known to be highly active catalysts for the Selective Catalytic Reduction (SCR) of NOx using NH_3 as a reductant.[1] Operating temperatures for maximum NOx conversion range between 300 and 450 °C and the technology is typically employed for stationary NOx abatement but since 2005 in Europe the technology has been employed commercially in heavy-duty mobile applications. In order to enhance both activity and stability they are normally 'promoted' to a significant extent (10 %) with group XVI elements such as Mo and W rendering the commercially applied catalysts as mixed phase $V_2O_5/(WO_3$ or $MoO_3)/TiO_2$. Much research has been undertaken in order to elucidate both the mechanism and active phase of the catalyst and it appears that there is general consensus on both; from an active phase perspective it has been proposed that both the VO_x and WO_x species are well spread over the TiO_2 support with O from the V-O-Ti/V-O-V of polymeric vanadates thought to be critical for activity at low temperatures.[2-7] In addition to enhanced deNOx activity the WO_x is proposed to have a number of additional benefits including the prevention of V polymerisation and volatilisation, the maintenance of the high surface area of the TiO_2 Anatase support and the offsetting of the first order solid-state phase transition to the TiO_2 Rutile phase with a much reduced surface area.[2, 8]

A major problem in catalytic application is deactivation. $V_2O_5/(WO_3$ or $MoO_3)/TiO_2$ catalysts are known to be generally resistant to chemical poisoning by SO_2 since the TiO_2 support is weakly and therefore reversibly sulfated. However thermal deactivation is a major problem for emission control catalysts, particularly when used in mobile applications since temperature spikes caused by running rich in fuel or air can mean that the catalyst experiences temperatures as great as 700-800 °C. Such high temperatures are known to cause sintering, phase transformation of TiO_2 Anatase to TiO_2 Rutile at temperatures > 600 °C and potentially volatalisation of vanadia; the melting point of pure V_2O_5 is 670 °C.

In this paper we demonstrate the results of a new, thermally stable V-SCR catalyst based on tailored silica stabilized raw materials and preparation methods when compared against the

conventional reference V-SCR catalyst based on pure anatase titania with the equivalent amount of vanadium and tungsten We examine then the effects of thermal aging of the two catalysts (a reference and an SiO_2-stabilised thermally durable type) at various temperatures before performing a detailed characterisation in order to examine how these temperature extremes lead to deactivation of the catalyst.

3. Experimental

3.1 Catalyst preparation

Two types of V-SCR samples were prepared: a conventional (reference) vanadium SCR catalyst (VSCR1) and a thermally stabilized (VSCR2) catalyst that contains about 4-5 wt-% silica demonstrated to act as a stabilizer and the resultant catalyst has been prepared in a way so as to produce a well-dispersed, high surface area containing stable catalyst.[9, 10] Vanadium SCR catalysts are based on pre-blended amorphous SiO_2 stabilized TiO_2 (Anatase) powder material, which is mixed in an aqueous slurry, where tungsten oxide (WO_x) and vanadium oxide (VO_x) are added dissolved in de-ionised water solutions of ammonium metavanadate (NH_4VO_3) and ammonium metatungstate hydrate $(NH_4)_6H_2W_{12}O_{40}.xH_2O$ precursors and left to homogenise for 1 h. The mixed acidic slurry was coated on a metallic substrate (thickness 50 µm, cell density 600 cells per in^2) and the coated catalyst was dried about at 80°C and calcinated at 550°C for 4 hours. The loadings of vanadium as coating used are 2.2 wt-% (calculated based on V_2O_5) and 10 wt-% tungsten (calculated based on WO_3).

3.2 Catalyst aging protocol

Catalysts were aged in situ in static air at 600, 700 and 800 °C for 3 h before being removed from the metallic substrate to powder samples for characterisation purposes so as to investigate how/whether such temperatures lead to thermally-induced phase transformation/sintering and concordant changes in surface area. Therefore, the preparation and ageing in this study were based on real structured catalysts, having a direct linkage to real catalysts in production, oppositely if preparing samples as powders only. The

fresh honeycomb samples were also hydrothermally aged at 650 and 700°C for 20 hours in a flow of 10 % water in air and comparative catalytic activity measurements made.

3.3 Catalyst characterisation

The surface area and pore size distribution were measured using the BET (Brunauer-Emmet-Teller) method with nitrogen adsorption-desorption isotherms (Sorptomatic 1990). NH_3 adsorption-desorption studies were performed by first adsorbing NH_3 first at 200 °C via a step exchange experiment ($0 \rightarrow 500$ ppm NH_3 in nitrogen, 42000 h^{-1}) followed by desorption of NH_3 in the presence of oxygen (TPO, Temperature Programmed Oxidation, 20 °C/min, 10 % O_2 in N_2. The reactor products were analysed using a Gasmet FTIR analyzer during a thermal ramping up to 600 °C. The ammonia adsorption capacity at 200 °C was calculated by the integration of NH_3 consumption during the step exchange response.

XAFS (XANES) were recorded on the Dutch-Belgian beamline (DUBBLE; BM26A) at the ESRF and B18 @ the Diamond Light Source.[11] Data were collected using a Si(111) double crystal monochromator with harmonic rejection achieved using the appropriate optics. V K-edge (5656 keV) measurements on the samples were performed in fluorescence mode using a 9-element monolithic germanium detector. Transmission measurements were performed on the crystalline oxide reference samples (V_2O_5, VO_2 and V_2O_3) and a 10 µm V foil to calibrate the monochromator position. In a typical experiment, approximately 100 mg sample was pressed to form self-supporting wafers before being mounted in air. Measurements were performed at room temperature in normal step-scanning mode over the range of 5420−5620 eV. A typical XANES spectrum was collected over a period of 30 min and at least 3 scans were performed for each sample. XANES data were processed using the using Athena (IFFEFIT software package).[12, 13] The XANES spectra were normalized from 30 to 150 eV above the edge energy, using a quadratic polynomial regressed through the data above the edge and extrapolated back to E_0. The extrapolated value of the post edge polynomial at E_0 is used as the normalisation constant.

XRD data were recorded on a Bruker D8 diffractometer with Bragg-Brentano geometry in flat plate mode using a Co $K_{\alpha+\beta}$ radiation source and rotating sample holder. Data were

recorded from 10 – 90 ° 2θ using a step size of 0.02 °/1 s acquisition time. XRD profile fitting to extract quantitative phase analysis (QPA) information of the final phase composition for the various samples was obtained using the Rietveld method. In order to do this the Powdercell programme was used to profile data over a 2θ range of 10 – 80 ° with no excluded regions. The background was simulated using a polynomial function whereas the diffraction peaks were profiled using a pseudo-voigt function and the atom positions and B iso values were fixed in order to enable the refinement to converge. Included in the final refinement were scale factors (and therefore the % age of each phase present), profile parameters, cell parameters and the zero-shift. Typical refined Rwp values ranged from 5.25 – 7.30 %. The obtained compositions were refined with a precision/accuracy of 5-10 % (depending on the number of phases present) of their actual weight percent. An example experimental pattern, as well as the fitted profiles and residuals are presented in ESI Figure Fig 2. [14] For particle size estimations using the Scherrer equation an instrument broadening function was first calculated using crystalline LaB_6 as a reference material.[15]

Raman data were recorded on self-supported wafers using a Kasier Optics instrument with a 5.5 inch objective lense (200 µm spot size) in backscatter mode with a 532 nm laser operating at 15 mW power and a CCD camera to record the data. The acquisition time employed was 10 s/spectra with 10 accumulations performed per sample with a total acquisition time of 5 min (inc. equivalent dark time acquisition). All Raman spectra were offset-corrected using Thermo Galactic Grams AI v. 7.0 software.

UV-Vis data were recorded in diffuse reflectance mode using a Cary-50 instrument with an acquisition time of 1 min/spectrum. 5 spectra were acquired and summed per sample with a dark and MgO reference used for calibration purposes.

X-ray Photoelectron spectroscopy (XPS) was carried out with a Thermo K-alpha instrument using monochromated Al Kα (1486.6 eV) radiation. Charge compensation was achieved using a dual mode (electron and Ar^+) flood gun, and spectra were referenced to adventitious Carbon 1s peak set to 285.0 eV. The V 2p region was fitted with Gaussian-Lorentzian line shapes on a Shirly background.

3.4 Catalyst activity measurements

The activity of SCR catalysts was investigated by steady state experiments between 150 – 600 °C in a quartz reactor tube mounted in an IR furnace.[16] The inlet concentration in the standard mixture was stoichiometric using NH_3/NO_x = 1: 1000 ppm NO_x (NO only or NO_2:NO = 400:600 ppm), 10 % O_2, 10 % H_2O, and balance nitrogen with space velocity (SV) of 50000 h^{-1}. The inclusion of NO_2 in the feed simulated the presence of a Pt oxidation catalyst before the SCR unit as is typically encountered in the mobile emissions system. [17, 18]

The gas compositions were analyzed with FTIR (Gasmet CR 2000) equipped with heated (180 °C) sampling lines, which prevents ammonia and water adsorption/condensation on the transfer lines.

4. Results and Discussion

4.1 SCR activity

The catalytic performance of both thermally aged VSCR1 and VSCR2 catalysts was examined in the Standard SCR (NO_2/NO_x = 0) and Fast SCR (NO_2/NO_x = 0.4) reactions, as shown in Figures 1 and 2, respectively.

After thermal ageing at 600 °C, VSCR1 still maintained reasonable Standard SCR activity (> 90 %) at 350 – 450 °C, which began to decline however, at higher temperatures, reaching ~ 38 % at 550 °C (Figure 1). In contrast NH_3 conversion increased with increasing reaction temperature (> 95 % at 450 – 600 °C), resulting in a ratio between converted NO_x and converted NH_3 less than 1. This implies that part of the NH_3 is not consumed during the SCR process and that is converted following a different reaction, probably by direct oxidation with oxygen:[19]

$$2NH_3 + {}^3/_2\, O_2 \rightarrow N_2 + 3H_2O \qquad (1)$$

$$2NH_3 + 2O_2 \rightarrow N_2O + 3H_2O \qquad (2)$$

$$2NH_3 + {}^5/_2\, O_2 \rightarrow 2NO + 3H_2O \qquad (3)$$

Above 377 – 427 °C, reactions (1)-(3) become competitive with the Standard SCR, decreasing the amount of available NH_3 and/or producing undesired NO or N_2O. In line with the NH_3

conversion data, increased amounts of N_2O (> 6 ppm) were produced over the VSCR1 catalyst at reaction temperatures higher than 450 °C, most likely through reaction (2).

Upon more severe ageing treatments, VSCR1 catalysts showed a strong decrease in SCR activity, along with a drop in NH_3 conversion, especially evident for the sample aged at 800 °C. A pronounced imbalanced conversion of NO_x and NH_3 was observed at high reaction temperatures (> 450 °C), more marked with increasing ageing temperature, leading to negative NO_x conversions above 500 °C. Furthermore, considerable amounts of N_2O were formed over the aged VSCR1 catalysts. For the sample treated at 800 °C, an important decrease in the ratio between converted NO_x and NH_3 was observed ($X_{NOx}/X_{NH3} < 1$ over the whole temperature range) however, only small amounts of N_2O (~ 4 % at 600 °C) were formed on this catalyst, suggesting that NH_3 was mainly oxidised to NO according to equation (3). Hydrothermal treatments caused a more significant effect on the catalytic performance of VSCR1. The hydrothermally aged samples exhibited a much important drop in activity, together with a considerable decrease in the ratio between converted NO_x and converted NH_3 above 450 °C. In accordance, larger amounts of N_2O were produced over these catalysts.

VSCR2 samples presented an enhanced stability as compared to VSCR1. As seen in Figure 1, the VSCR2 catalysts maintained a relatively high activity under standard SCR conditions, together with a higher N_2 selectivity than VSCR1 samples. Ageing at 800 °C also lead to an important loss in activity and selectivity, but less pronounced than for VSCR1. Importantly, VSCR2 catalysts exhibited a much better tolerance to hydrothermal treatments, with HT650 and HT700 samples presenting a high level of NO_x conversion (> 90 %) at 350 – 450 °C. The hydrothermally aged VSCR2 samples showed as well a reduced NH_3 oxidation activity and a less pronounced unbalanced conversion of NO_x and NH_3. In contrast to VSCR1 catalysts, VSCR2 were more resistant to hydrothermal than to thermal treatments.

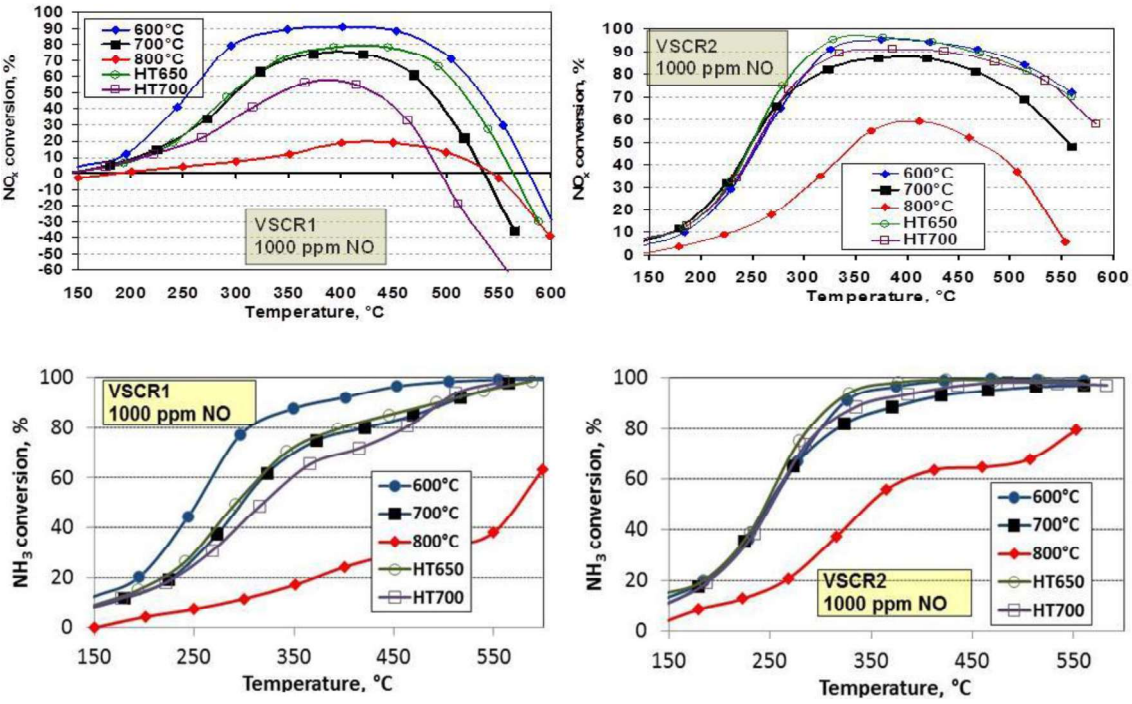

Figure 1. *Standard SCR activities and NH_3 conversion data of both thermally and hydrothermally aged VSCR1 and VSCR2 samples, using a GHSV of 50000 h^{-1} and a feed composition of 1000 ppm NO, 1000 ppm NH_3, 10 % O_2 and 10 % H_2O.*

As seen in Figure 2, both VSCR1 and VSCR2 catalysts showed an enhancement in the activity at low temperatures under Fast SCR conditions. This is related with the V redox properties, which lead to a higher deNO_x efficiency.[20] Similarly to the Standard SCR, all VSCR2 catalysts presented much better stability than VSCR1, maintaining a high level of NO_x conversion (> 90 % at 350-450 °C) even upon ageing at 700 °C. Again, VSCR1 samples exhibited a gradual drop in activity with increasing ageing temperature, as well as negative NO_x conversions above 500 °C (see ESI Figure 1). Furthermore, as previously observed, VSCR2 catalysts displayed an improved stability towards hydrothermal ageing, more evident than under Standard conditions.

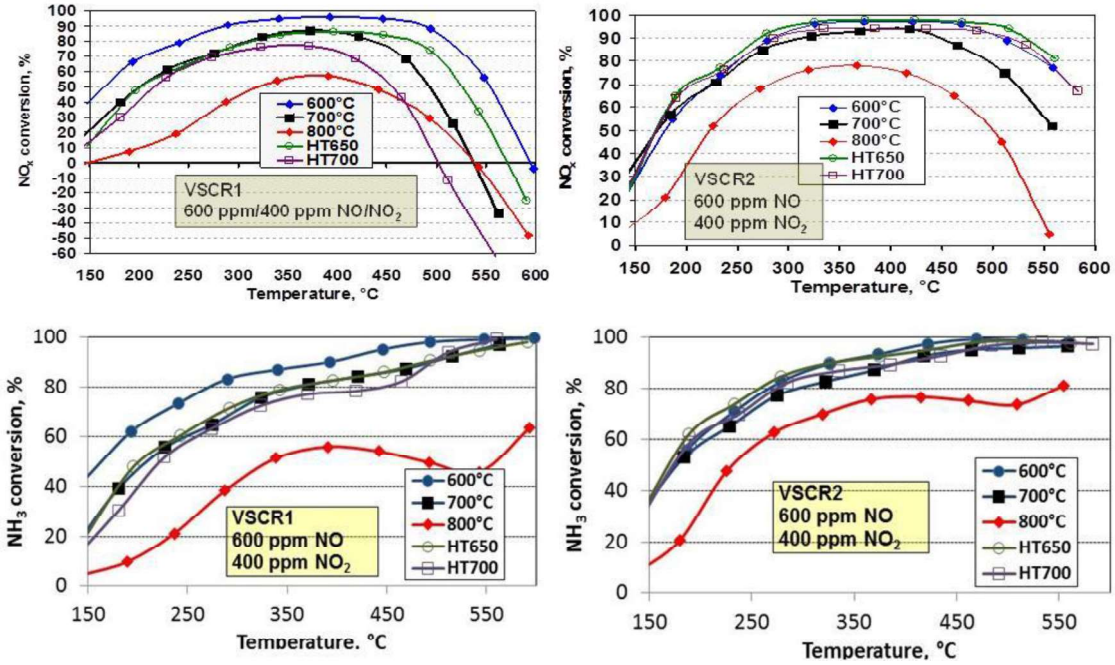

Figure 2. *Fast SCR activities and NH_3 conversion data of both thermally and hydrothermally aged VSCR1 and VSCR2 samples, using a GHSV of 50000 h^{-1} and a feed composition of 600 ppm NO, 400 ppm NO_2, 1000 ppm NH_3, 10 % O_2 and 10 % H_2O*

4.2 Surface area and ammonia adsorption capacity

The BET specific surface area studies for the thermally aged samples are given in Figure 3. The reduction in surface area with increasing temperature indicated that morphological changes, which have an effect on the stability of V and W compounds on the porous TiO_2 surface, have taken place. The surface area of a newly prepared sample is typically 80 – 100 m^2/g for both samples but drops then with the ageing temperature.[16] Whilst VSCR1 loses a part of the surface area already at 600 °C, stabilized VSCR2 retains most of its surface area at this temperature (Figure 3). A critical surface area is thought to about 50 m^2/g which is sufficient to maintain enough surface and to keep V and W compounds stable for SCR reactions [15]. Hydrothermal treatment at 700°C led to severe loss of surface area (10 m^2/g) for VSCR1, which correlated also to the drop in SCR activity seen in Figures 1 and 2. The pore volume related to N_2 adsorption-desorption isotherm correlated also to the changes in BET surface.

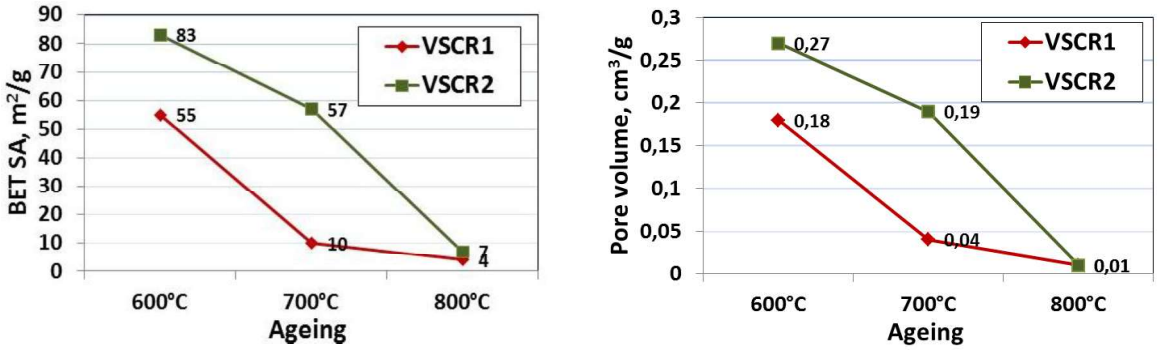

Figure 3. *BET surface area and pore volumes of VSCR catalysts by N_2 adsorption-desorption isotherms at -196°C as a function of ageing temperature.*

Ammonia adsorption capacity is a property related to SCR functionality adsorbing on both Brønsted and Lewis acid sites. It has previously been shown that ammonia adsorbed on Brønsted acid sites play a role in the vanadium catalysed SCR process at low temperatures (< 300 °C) but less so at temperatures > 400 °C.[21] Ammonia adsorption measurement at 200 °C showed that the total acidity of catalyst surface mimics the drop seen in the surface area shown in Figure 3 – note that the NH_3 adsorption capacity of both these catalysts are initially > 100 µmol/g.[16] Ageing at 800 °C destroys the surface (and its acidic properties) on both VSCR catalysts, although a clear effect of stabilization in the VSCR2 catalyst can be seen at the critical temperature at 700 °C.

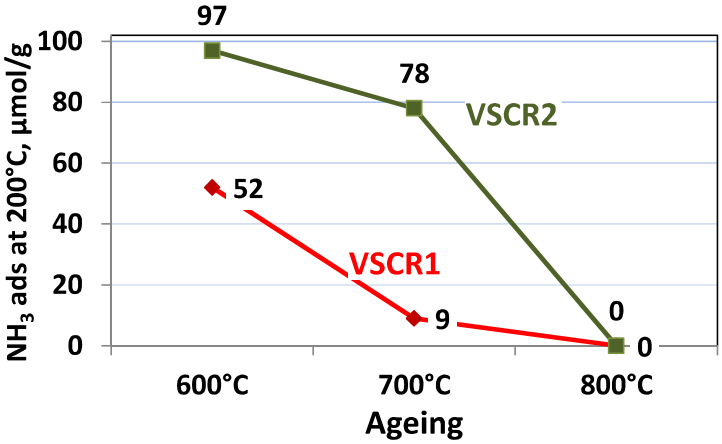

Figure 4. *Ammonia adsorption capacity at 200 °C on VSCR catalysts as a function of ageing temperature.*

4.3 XRD data

XRD data for both catalysts after thermal aging are given in Figure 5 and ESI Figure 2 respectively and revealed that all samples are highly crystalline with the main reflections ascribable to the presence of either TiO_2 Anatase or Rutile (see ESI Table 1). After treatment at 600 °C this is the only phase present in both samples. The rather broad but clear reflections corresponding to the (101), (200) were used for performing a Scherrer analysis and suggested that the TiO_2 particles to be ~ 16 – 18 nm – the similarity of the particle size estimation suggesting also that the particles are reasonably isotropic.[22] Heat treatment at 700 °C lead to a small degree of sintering (slightly anisotropic) of the TiO_2 Anatase phase as evidenced by growth of the (111) reflection (~ 30 % more intense) than that seen at 600 °C. Treatment at 800 °C lead to the formation of small amounts (~20 % by weight) of TiO_2 Rutile. Sintering of the TiO_2 Anatase phase is now severe (particles > 100 nm) and in addition peaks due to monoclinic WO_3 are now also present. The results from a multiple phase Lebail extraction performed on the samples treated at 700 and 800 °C are shown in Table 1.

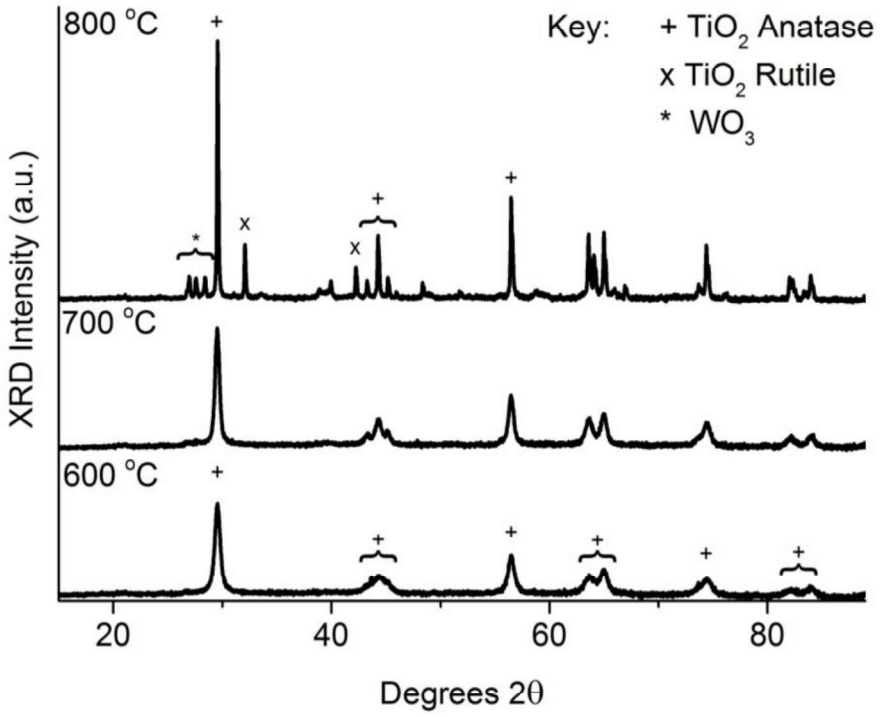

Figure 5. *XRD data with VSCR2 with increasing temperature of thermal treatment. The important Bragg peaks for the respective phases TiO_2 Anatase, TiO_2 Rutile and monoclinic WO_3 have been identified with a **+**, **x** or ***** accordingly. Table 1 in the ESI contains a list of the seven most pertinent reflections of each phase present.*

For the XRD data of VSCR1 revealed all samples to be highly crystalline. The sample aged at 600 °C contained reflections ascribable to TiO_2 Anatase possessing anisotropic crystallites greater in size than that seen for VSCR2. The sample aged at 700 °C contains also clear evidence of TiO_2 Anatase although the intensity of this signal is greater (~ 100 % more intense) than that seen at 600 °C suggesting further growth/sintering of this phase; the average particle size observed now being >> 100 nm in size. Also now present in the pattern are reflections due to TiO_2 Rutile as well as the appearance of Bragg peaks due to the formation of monoclinic WO_3 crystallites as a result of phase segregation. VSCR1 aged at 800 °C is by contrast completely dominated by the presence of TiO_2 Rutile which also undergoes significant sintering between 700 and 800 °C. Also present in the pattern are peaks for TiO_2 Rutile and again clear evidence for monoclinic WO_3. From ESI Figure 4, the characteristics of the WO_3 phase do not however change particularly on heating to 800 °C. The results from a multiple phase Lebail extraction performed on the samples aged at 800 °C are shown in Table 1. Rutile fraction was about 20 wt-% on VSCR1 aged at 700°C and on VSCR2 aged at 800°C, showing an improved thermal stability of about 100°C between these two coatings.

Table 1. *Phase composition (mass %) for crystalline phases present in VSCR1 and VSCR2 determined from a full pattern Lebail fitting.*

Sample	Mass % Anatase	Mass % Rutile	Mass % WO_3
VSCR1-700	73.2	20.9	5.9
VSCR1-800	6.5	91.5	1.9
VSCR2-800	75.9	19.9	4.2

**The only crystalline phase present in VSCR1-600, VSCR2-600 and VSCR-2-700 is TiO_2 Anatase*

The XRD data and in particular the large TiO_2 crystallites demonstrate that the decrease in the surface area and pore volume seen in Figures 3 and 4 occur due to severe sintering and phase transformation of the TiO_2 crystallites.

4.4 Raman

Raman spectra obtained from the samples correspond well with the XRD data, containing strong well-defined bands for TiO_2 Anatase phase (see Table 2 and Figures 6 and ESI Figure 5

for further details and assignments) or in the VSCR1-800 °C sample, Rutile.[23] With increased temperature treatment the TiO_2 Anatase bands become both more narrow and weaker as the phase sinters and eventually transforms into TiO_2 Rutile. The sintering of TiO_2 Anatase affects the intensity/peak widths of the A_{1g} and B_{1g} modes more dramatically than the E_g mode and suggests the sintering to be non-uniform. In addition to the TiO_2 phases weak bands between 804 – 807 cm^{-1} can be seen ascribable to the υ (O-W-O) mode of monoclinic WO_3; in instances where the WO_3 phase is particularly crystalline (i.e. after heat treatment at 700 – 800 °C the υ (W-O) band at ~ 712 cm^{-1} can also be seen).[24] Evidence for the presence of presence of vanadium in the form of polymeric V_2O_5 likely dispersed over the WO_3 surface can also be seen by virtue of the band at ~ 985 cm^{-1}.[2, 25] Weak bands ~ 930 cm^{-1} also suggest the presence of V_xO_y species.[26] The absence of bands > 1000 cm^{-1} suggests that V=O species often associated with isolated V^{5+} species are not present to any great extent; however it is debateable whether such bands are visible unless measurements are made in the absence of water (dehydrated).[5] After treatment at higher temperatures however the weak bands at ~ 930 cm^{-1} followed by the 985 cm^{-1} band disappear suggesting disappearance of the V_2O_5 polymeric species. However no clear evidence for an alternative vanadium containing phase could be seen from either Raman or XRD.

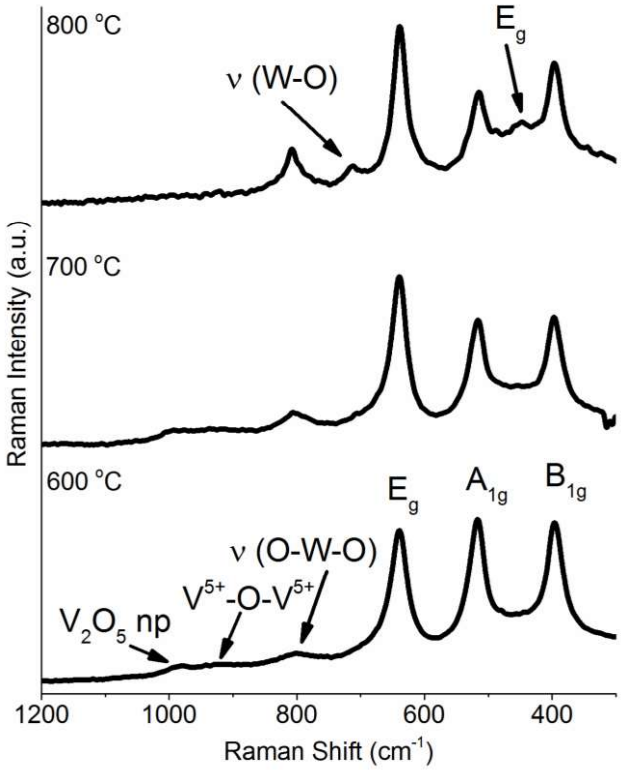

Figure 6. *Raman data from VSCR2 with increasing temperature of thermal treatment. The band assignments and results from the peak profiling are illustrated and are also listed in Table 2. The E_g band in the sample aged at 800 ^oC originates from TiO_2 Rutile.*

4.5 UV-Vis data

The presence of TiO_2 (both Anatase and Rutile forms) in large amounts is also evident from the UV-Vis spectra (Figure 7 and ESI Figure 6). The major features therefore comprise the ligand-to-metal charge transfer (LMCT) bands at 230-350 nm associated with TiO_6 species in the TiO_2 Anatase and Rutile forms.[27] A pale yellow hue to the samples suggests the presence of V^{5+} (possible polymeric V_2O_5-type species as seen by Raman scattering) are also present although the contribution to this component is somewhat difficult to unambiguously discern against the TiO_2 'background'.[28] At higher temperatures the samples become increasingly darker (increased absorption in the visible region) suggestive of both a reduction in the amount of TiO_2 Anatase phase present (concurrent increase in the amount of TiO_2 Rutile as evidenced by the bands ~ 350 nm) and reduction of the initial V species. This increased absorption in the visible region between 420 – 700 nm has previously been ascribed to polymerisation of V^{5+} containing VO_x species on the catalyst

surface. No confirmatory evidence for this could be found in the Raman spectrum for V_2O_5 nanoparticles or bulk species. Most likely then such a change should be interpreted in terms of a reduction of V^{5+} species to either V^{4+} or V^{3+}containing species.

Table 2. *Raman bands and fitted position, width and intensities for the various samples after thermal treatment.*

Sample	Band/Vibration origin	Position (cm^{-1})	Band width (cm^{-1})	Relative Band intensity (a.u.)
VSCR2 (600 °C)	(TiO_2) Anatase (B_{1g})	396	34	0.84
	(A_{1g})	517	34	0.996
	(E_g)	639	31	1
	υ (O-W-O)	804	46	0.06
	V^{5+}-O-V^{5+}	928	54	0.03
	V_2O_5 polymeric	985	28	0.04
VSCR2 (700 °C)	(TiO_2) Anatase (B_{1g})	396	29	0.63
	(A_{1g})	517	28	0.63
	(E_g)	640	29	1
	υ (O-W-O)	804	47	0.07
	V^{5+}-O-V^{5+}	928	55	0.04
	V_2O_5 polymeric	985	103	0.07
VSCR2 (800 °C)	(TiO_2) Anatase (B_{1g})	396	27	0.59
	(A_{1g})	517	26	0.44
	(E_g)	640	25	1
	υ (W-O)	712	18	0.09
	υ (O-W-O)	807	30	0.24
VSCR1 (600 °C)	(TiO_2) Anatase (B_{1g})	396	26	0.73
	(A_{1g})	517	28	0.76
	(E_g)	639	30	1
	υ (O-W-O)	804	125	0.08
	V^{5+}-O-V^{5+}	930	49	0.04
	V_2O_5 polymeric	985	22	0.05
VSCR1 (700 °C)	(TiO_2) Anatase (B_{1g})	396	34	0.55
	(A_{1g}) 516	516	28	0.45
	(E_g) 639	639	28	1
	υ (O-W-O) 804	804	41	0.18
VSCR1 (800 °C)	(TiO_2) Rutile (E_g)	449	95	1
	(A_{1g})	610	43	0.69
	υ (W-O)	713	36	0.1
	υ (O-W-O)	807	55	0.25

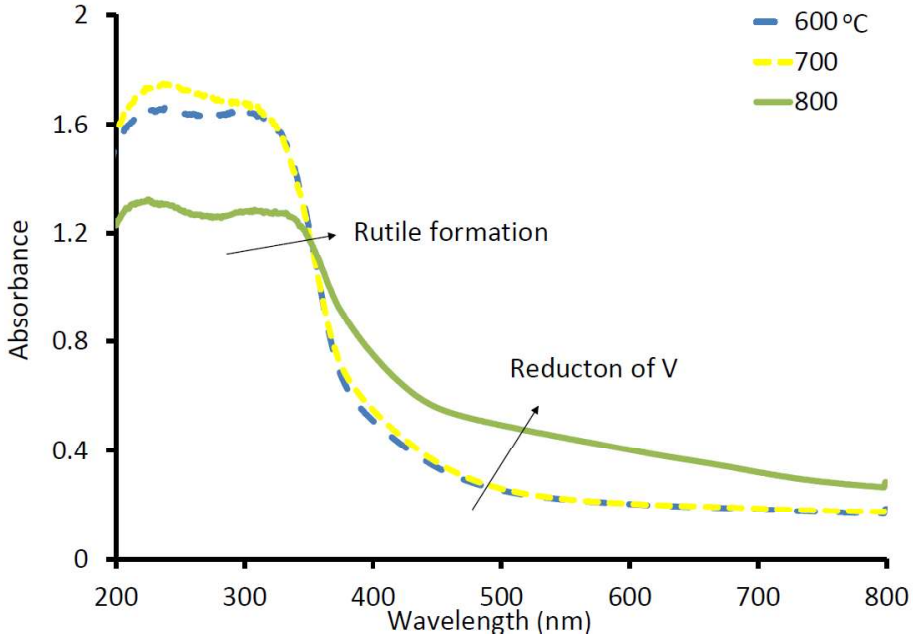

Figure 7. *UV-Vis spectra for VSCR2 with increasing temperature of thermal ageing. The arrows indicate the shifts in either the LMCT band position (due to TiO_2 Rutile formation) or else the increased absorption in the visible region due to reduction of V species. The LMCT bands present in the spectra are listed in Table 3.*

Table 3. *Centroid band position of the LMCT bands from the UV-Vis spectra shown in Figure 3 and ESI Figure 5.*

Sample	LMCT band positions (nm)
VSCR1 600 °C	237 and 296 nm
VSCR1 700 °C	234 and 304 nm
VSCR1 800 °C	244 and 348 nm
VSCR2 600 °C	241 and 296 nm
VSCR2 700 °C	238 and 298 nm
VSCR2 800 °C	224 and 308 nm

4.6 XANES and XPS data

V K-edge XANES data are shown in Figure 8 for VSCR2 whilst reference spectra for the VSCR1 series and reference spectra for V^{5+} to V^{3+} containing reference oxides are shown in ESI Figure 7 . There appears much debate in the literature as to which features in the XANES spectra can be used to determine the oxidation and coordination state and therefore the nature V species in solid phases.[29-31] Attempts have been made to correlate the position, width and/or intensity of the pre-edge peak much in the same way as has been done successfully for Ti and Fe containing compounds although the richer redox and local structure variation for the V compounds has demonstrated that this is more difficult.[32, 33]

The key features for the V K-edge XANES spectra have been highlighted with arrows in Figure 8 and ESI Figure 7 and include the pre-edge peak due to the 1s-3d dipole transition, the edge position (E_0) and the rising absorption edge dominated by the dipole allowed 1s-4p transition. It is clear that changes in all three regions occur with increasing ageing temperature; broadly these changes involve a reduction in the pre-edge peak intensity, a positive (in energy) shift in the E_0 position and an increase in the rising absorption edge. These key observations and their interpretation from the samples are given in Table 4. A simple comparison of the XANES spectra for the samples with those for the reference compounds (ESI Figure 7) suggested that the end members of the sample series (i.e. samples treated at 600 and 800 ^{o}C) to possess V environments similar to V_2O_5 and V_2O_3 respectively. In particular the samples treated at 800 ^{o}C look almost identical to the V_2O_3 reference spectrum. Furthermore the XANES spectra from the samples treated at intermediate temperatures can be rationalised as comprising a mixture of V_2O_5 and V_2O_3, consistent with the Raman and UV-Vis results. We propose to use a straightforward approach of comparison of edge position (E_0 typically found around ~ 5480 eV and in this case we determined the edge position from 50 % of the normalised intensity) as a method to determine average oxidation state in the samples since the likely V species present will probably resemble the oxide reference compounds V_2O_5, VO_2 and V_2O_3. These reference compounds have also been measured and used to create a calibration curve (ESI Figure 8) from which the average oxidation state of the V containing phases on supported catalysts can be estimated. Whilst this approach works well for oxidation state determination, it does not tell us much about the coordination state of the species present. Here we need to consider the full XANES spectrum to determine whether multiple V^{5+} species species/environments are present in the sample. Using a combination of the XANES data recorded for the oxide references (and observations made with Raman and UV-Vis) and the previous work of Boyesen et al. we conclude that the initial VSCR1/VSCR2 catalyst contain predominantly polymeric V_2O_5 species but that a reduced pre-edge peak intensity (0.41/0.45) in comparison to the V_2O_5 (0.46) suggests that there are either a small amount of octahedrally coordinated monomeric V^{5+} species or else that these monomeric V^{5+} species undergo a 'structural distortion' as a result of a coordinating water ligand (see ESI Figure 8 for a comparative plot).[28, 31] The lower pre-edge peak intensity for the VSCR1 sample suggests that there are slightly more of these octahedral species present in

comparison to VSCR2. Both the pre-edge peaks in VSCR1 and VSCR2 are slightly wider than that of the V_2O_5 crystalline reference sample suggesting a wider V-O bond distance variation, consistent with the presence of non-crystalline V_2O_5 species being present.[34] Although there appears little evidence for VO_2 in the samples from the bulk measurements it appears from the XPS data shown in Table ESI 3 that V^{4+} species may be present in the sample although concentrated at the surface. In fact all samples contained surfaces rich in reasonably equivalent amounts of $V^{4+/5+}$ species even though the bulk of the samples tended to be dominated by either V^{5+} or V^{3+} species.

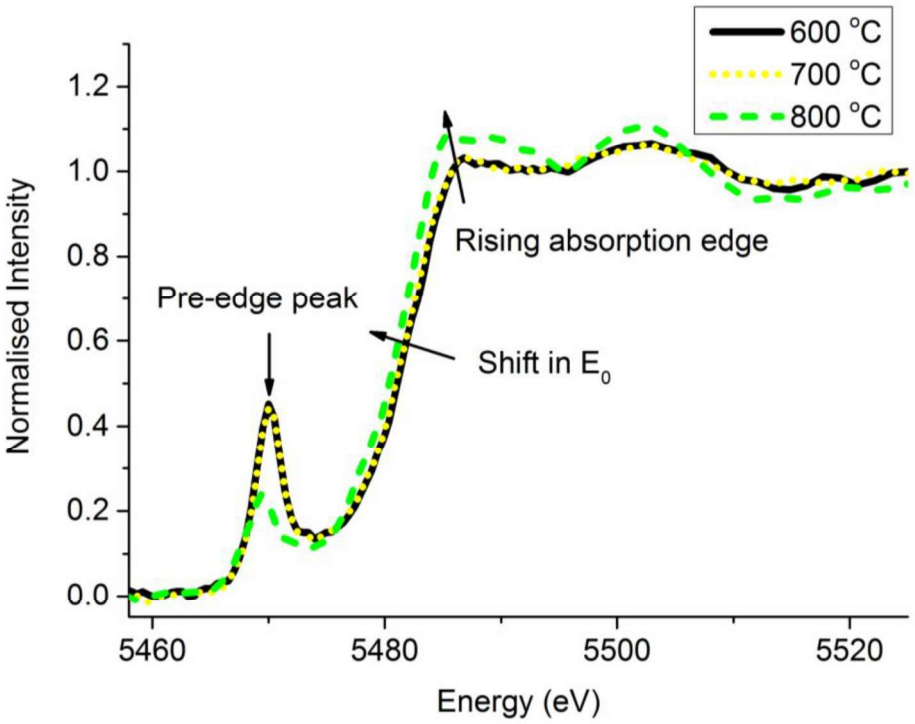

Figure 8. *XANES spectra for VSCR2 after ageing at three different temperatures. The key features including the pre-edge peak, E_0 position and the rising absorption edge and their tendency with increasing treatment temperature have been highlighted using arrows.*

5. Summary

Both V_2O_5/WO_3-$TiO_2(SiO_2)$ catalysts after thermal aging at 600 °C still possess the essential characteristics that render them active for NH_3-SCR; Raman spectroscopy and V K-edge XANES measurements (and to some extent the absence of Bragg diffraction) point towards the presence of polymeric V_2O_5 being the predominant V^{5+} containing species present. These results are consistent with previous observations that these polymeric V species are more active for NOx conversion than isolated V sites, although it has been reported that are

somewhat less selective towards N_2, especially at high temperatures.[35, 36] Critically it appears that SCR activity increases with increasing V content up to monolayer surface coverage, decreasing after that owing to the formation of microcrystalline V_2O_5 particles. [35-37] Selectivity to N_2 is also affected by the formation of bulk V_2O_5. [37-39] Raman spectroscopy also reveals that well-dispersed WO_3 species are present in these samples most likely supporting/stabilising the well-dispersed V_2O_5 species according to recent research. Finally the V_2O_5 polymeric species/WO_3 are well dispersed over the Anatase TiO_2 and SiO_2-stabilised TiO_2 crystallites < 20 nm in size. [25, 40]

Table 4. *Pre-edge peak position, intensity, edge position (50 % of the normalised intensity) and oxidation state determined for various V-containing oxide references and for the series of hydrothermally aged samples.*

Sample	Pre-edge peak position (eV)	Pre-edge peak intensity	E_0 (eV)	Oxidation state (average)
V_2O_5	5470.0	0.46	5481.1	5+
VO_2	5470.3	0.61	5480.6	4+
V_2O_3	5469.0	0.23	5479.0	3+
VSCR1 600 °C	5470.0	0.41	5481.0	5+
VSCR1 700 °C	5469.6	0.29	5480.6	4+
VSCR1 800 °C	5469.0	0.17	5479.3	3.2+
VSCR2 600 °C	5470.0	0.45	5481.0	5+
VSCR2 700 °C	5470.0	0.45	5480.8	4.5+
VSCR2 800 °C	5469.5	0.24	5480.4	3.9+

The major impact on the system when heating to temperatures > 700 °C, particularly for the VSCR1 catalyst is first sintering of the TiO_2 (as determined by a drop in surface area and observation of larger crystallites (> 100 nm) by XRD) followed by the Anatase-to-Rutile phase transformation. This sintering, severe already after ageing at 700 °C, leads to phase segregation of the catalyst and in particular WO_3 which subsequently crystallises in the monoclinic form. Vanadium species are partially reduced (average valence from V K-edge XANES of 4.0) most likely as a result of partial phase segregation of the polymeric V_2O_5 species from the sintered catalyst and subsequent autothermal reduction. Heating to 800 °C sees further sintering of the TiO_2 Anatase and Rutile phases whilst further autothermal reduction takes place leading to the eventual formation of V_2O_3 species (according to UV-Vis and V K-edge XANES data). The presence of bands due to V_2O_3 in the Raman spectrum will be obscured by those due to TiO_2 Anatase and Rutile species, whilst the V loading is too low to detect crystallites. Although not characterised here we propose that it is likely that the

hydrothermally aged samples undergo a similar mechanism of deactivation i.e. phase-transformation/sintering process as previous results suggest. [16]

In contrast the SiO_2-stabilised VSCR2 catalyst exhibits similar sintering and phase segregation behaviour to VSCR1 although crucially this behaviour is offset. From the results of the characterisation performed here there are very few obvious differences in the nature of the V, WO_3 and TiO_2 species present in either VSCR1 or VSCR2 although, consistent with previous studies, this small amount of SiO_2 offsets sintering and the anatase-to-rutile phase transformation by ~100 °C.[9] In this previous work by Hirano et al. studying a range of SiO_2:TiO_2 composites found evidence, particularly in the highest loaded (48.2 mol %) SiO_2 composites, of an amorphous SiO_2 shell surrounding the outside of the anatase particles. Considering that the loadings used here are similar to the lower loadings used in the study by Hirano et al. it is therefore likely the same amorphpous SiO_2 shell is present in the samples studied here.

Specifically VSCR2 is more resistant to treatment at 700 °C (even in the presence of water) retaining much of the surface area present at 600 °C whilst also maintaining a significant proportion of Brønsted acidity and active polymeric V_2O_5 species (although an average oxidation state of 4.5 suggests some autothermal reduction takes place). Treatment at 800 °C does however lead to notable sintering, phase transformation, segregation and autothermal V reduction as seen in VSCR1 all leading to a reduced overall catalytic performance.

Figure 9 contains an overall summary of the impact of thermal treatment on the physical properties of the catalysts and their overall activity. With regards to the SCR reaction mechanism, we note that thermal ageing at 700 °C of the VSCR1 catalyst had a dramatic effect on both the ammonia adsorption capacity and the surface area of the TiO_2 support although NOx conversion remained at ~80 % of the conversion seen for VSCR1 treated at 600 °C. This suggested that the primary effect of thermal aging on NO conversion concerns the vanadium species and in particular that the loss of polymeric V_2O_5 species and formation of inactive bulk V_2O_3 probably leads to deactivation via a reduction in the number of available active sites and a hiatus in the sold-state redox cycle.

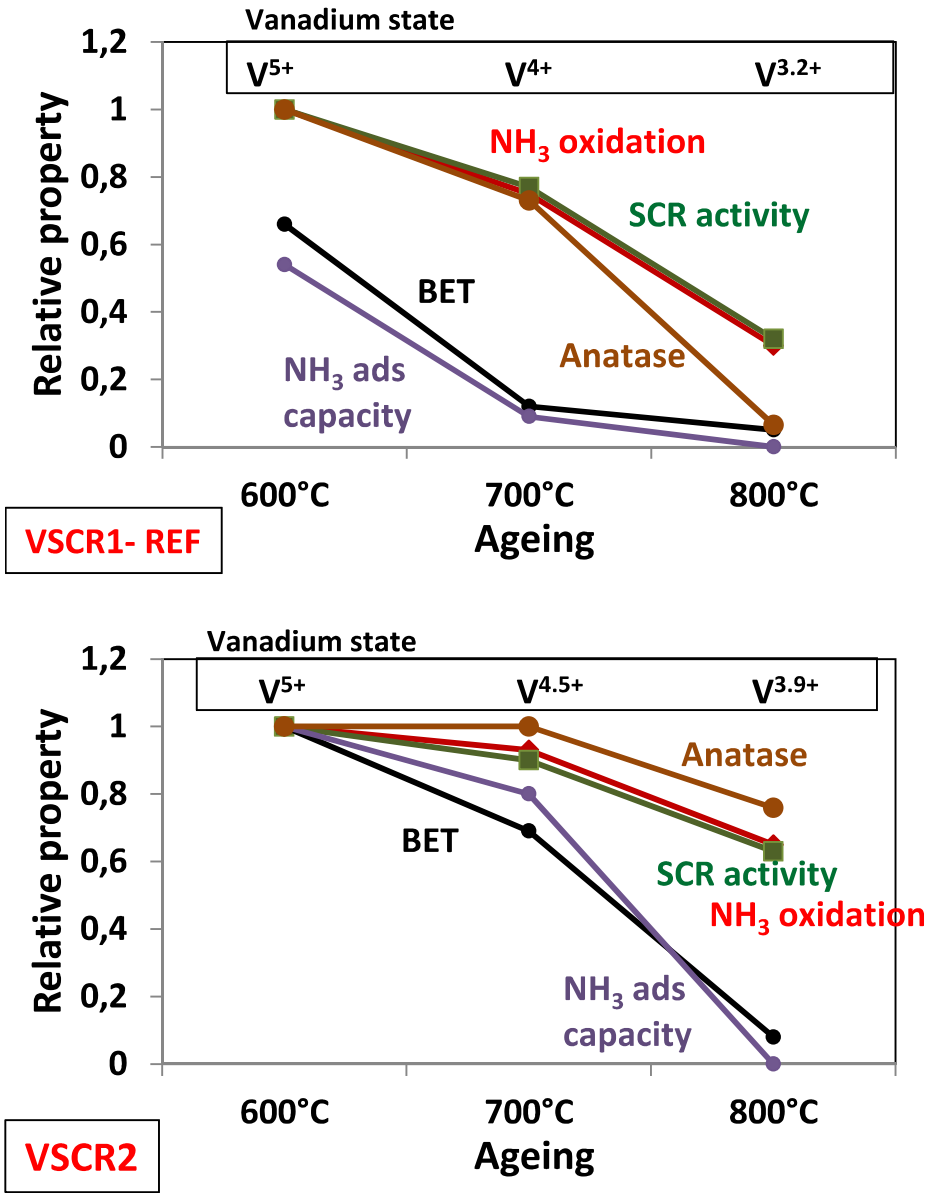

Figure 9. *Correlation graph illustrating the effect of thermal ageing treatment against the relative change in the measured variable (surface area, NH_3 adsorption capacity, crystalline phase, SCR activity and V oxidation state) of the VSCR1 and VSCR2 catalysts. Note that the values for the relative property are given with respect to the optimal value for the VSCR2 catalyst.*

6. Conclusions

The addition of small (~ %) amounts of stabilising agent together with the developed preparation methods has a significant effect on the thermal stability of an active V-SCR catalyst enabling it to withstand high operation temperatures and retain much of its catalytic activity. This study also demonstrates the importance of using multiple

characterisation techniques in conjunction with detailed catalytic testing to fully appreciate and understand the evolution of the structure of the supported catalyst with its catalytic function and thermal durability.

7. Acknowledgements

The authors are grateful to EPSRC and TEKES Finland in the FCEP research project for funding. We acknowledge the UK Catalysis BAG access to B18 of Diamond Light Source, EPSRC for funding support to Andrew M. Beale and I. Lezcano-Gonzalez and ESRF for access to BM26A.

8. References

[1] F. Liu, W. Shan, X. Shi, H. He, Progress in Chemistry, 24 (2012) 445-455.
[2] P.G.W.A. Kompio, A. Brueckner, F. Hipler, G. Auer, E. Loeffler, W. Gruenert, Journal of Catalysis, 286 (2012) 237-247.
[3] L.J. Alemany, L. Lietti, N. Ferlazzo, P. Forzatti, G. Busca, E. Giamello, F. Bregani, Journal of Catalysis, 155 (1995) 117-130.
[4] N.Y. Topsoe, J.A. Dumesic, H. Topsoe, Journal of Catalysis, 151 (1995) 241-252.
[5] I.E. Wachs, Dalton Transactions, 42 (2013) 11762-11769.
[6] B.M. Weckhuysen, D.E. Keller, Catalysis Today, 78 (2003) 25-46.
[7] I. Nova, L.D. Acqua, L. Lietti, E. Giamello, P. Forzatti, Applied Catalysis B-Environmental, 35 (2001) 31-42.
[8] A. Kubacka, A. Iglesias-Juez, M. di Michiel, A. Isabel Becerro, M. Fernandez-Garcia, Physical Chemistry Chemical Physics, 16 (2014) 19540-19549.
[9] M. Hirano, K. Ota, H. Iwata, Chemistry of Materials, 16 (2004) 3725-3732.
[10] A. Li, Y. Jin, D. Muggli, D.T. Pierce, H. Aranwela, G.K. Marasinghe, T. Knutson, G. Brockman, J.X. Zhao, Nanoscale, 5 (2013) 5854-5862.
[11] S. Nikitenko, A.M. Beale, A.M.J. van der Eerden, S.D.M. Jacques, O. Leynaud, M.G. O'Brien, D. Detollenaere, R. Kaptein, B.M. Weckhuysen, W. Bras, J. Synchrot. Radiat., 15 (2008) 632-640.
[12] M. Newville, J. Synchrot. Radiat., 8 (2001) 322-324.
[13] B. Ravel, M. Newville, J. Synchrot. Radiat., 12 (2005) 537-541.
[14] P. Ngene, P. Adelhelm, A.M. Beale, K.P. de Jong, P.E. de Jongh, J. Phys. Chem. C, 114 (2010) 6163-6168.
[15] U. Holzwarth, N. Gibson, Nature Nanotechnology, - 6 (2011) - 534.
[16] T. Maunula, T. Kinnunen, K. Kanniainen, A. Viitanen, A. Savimaki, SAE International, 2013-01-1063 (2013).
[17] G. Madia, M. Koebel, M. Elsener, A. Wokaun, Industrial & Engineering Chemistry Research, 41 (2002) 3512-3517.
[18] T. Maunula, R. Lylykangas, A. Lievonen, M. Harkonen, SAE International, 2003-01-91 (2003).
[19] G. Busca, L. Lietti, G. Ramis, F. Berti, Applied Catalysis B-Environmental, 18 (1998) 1-36.
[20] E. Tronconi, I. Nova, C. Ciardelli, D. Chatterjee, M. Weibel, Journal of Catalysis, 245 (2007) 1-10.
[21] N.Y. Topsoe, H. Topsoe, J.A. Dumesic, Journal of Catalysis, 151 (1995) 226-240.
[22] E.K. Gibson, M.W. Zandbergen, S.D.M. Jacques, C. Biao, R.J. Cernik, M.G. O'Brien, M. Di Michiel, B.M. Weckhuysen, A.M. Beale, Acs Catalysis, 3 (2013) 339-347.
[23] H.C. Choi, Y.M. Jung, S.B. Kim, Vibrational Spectroscopy, 37 (2005) 33-38.

[24] R.F. Garcia-Sanchez, T. Ahmido, D. Casimir, S. Baliga, P. Misra, Journal of Physical Chemistry A, 117 (2013) 13825-13831.
[25] C.A. Carrero, C.J. Keturakis, A. Orrego, R. Schomaecker, I.E. Wachs, Dalton Transactions, 42 (2013) 12644-12653.
[26] A. Bruckner, E. Kondratenko, Catalysis Today, 113 (2006) 16-24.
[27] J.G. Li, T. Ishigaki, X.D. Sun, J. Phys. Chem. C, 111 (2007) 4969-4976.
[28] X.T. Gao, S.R. Bare, J.L.G. Fierro, I.E. Wachs, Journal of Physical Chemistry B, 103 (1999) 618-629.
[29] J. Wong, F.W. Lytle, R.P. Messmer, D.H. Maylotte, Physical Review B, 30 (1984) 5596-5610.
[30] P. Chaurand, J. Rose, V. Briois, M. Salome, O. Proux, V. Nassif, L. Olivi, J. Susini, J.-L. Hazemann, J.-Y. Bottero, Journal of Physical Chemistry B, 111 (2007) 5101-5110.
[31] K.L. Boyesen, K. Mathisen, Catalysis Today, 229 (2014) 14-22.
[32] M. Wilke, F. Farges, P.E. Petit, G.E. Brown, F. Martin, American Mineralogist, 86 (2001) 714-730.
[33] F. Farges, G.E. Brown, J.J. Rehr, Physical Review B, 56 (1997) 1809-1819.
[34] K.L. Boyesen, F. Meneau, K. Mathisen, Phase Transitions, 84 (2011) 675-686.
[35] G.T. Went, L.J. Leu, A.T. Bell, Journal of Catalysis, 134 (1992) 479-491.
[36] I.E. Wachs, G. Deo, B.M. Weckhuysen, A. Andreini, M.A. Vuurman, M. deBoer, M.D. Amiridis, Journal of Catalysis, 161 (1996) 211-221.
[37] S. Djerad, L. Tifouti, M. Crocoll, W. Weisweiler, Journal of Molecular Catalysis a-Chemical, 208 (2004) 257-265.
[38] G. Madia, M. Elsener, M. Koebel, F. Raimondi, A. Wokaun, Applied Catalysis B-Environmental, 39 (2002) 181-190.
[39] O. Kroecher, M. Elsener, Applied Catalysis B-Environmental, 77 (2008) 215-227.
[40] A. Burkardt, W. Weisweiler, J.A.A. van den Tillaart, A. Schafer-Sindlinger, E.S. Lox, Topics in Catalysis, 16 (2001) 369-375.

Abstract graphic
Click here to download high resolution image

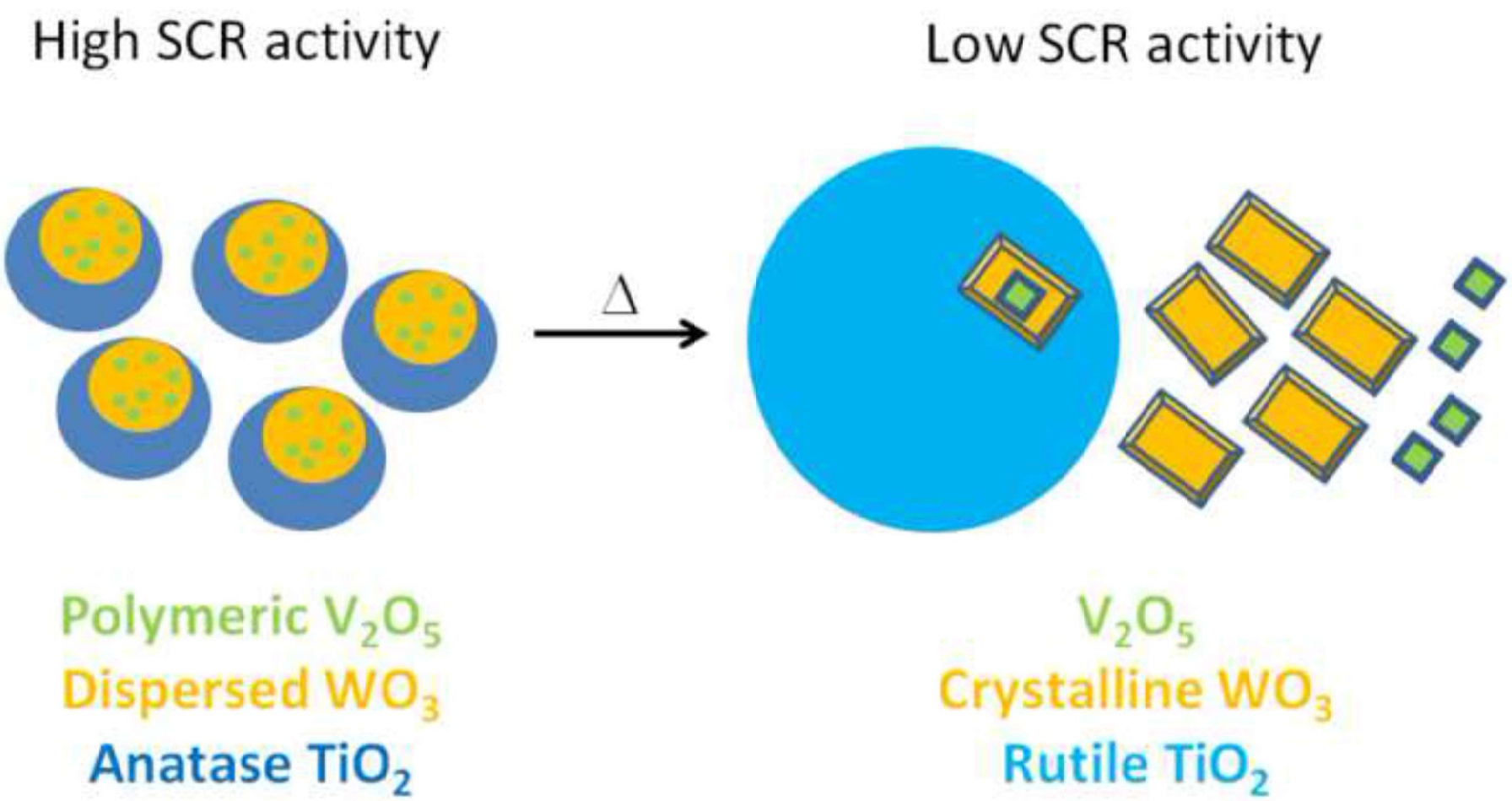

ESI For: Development and characterisation of thermally stable supported V-W-TiO_2 catalysts for mobile NH_3-SCR applications

Andrew M. Beale[a,b,c], I. Lezcano-Gonzalez [a,b], Teuvo Maunula[d], Robert G. Palgrave[a]

[a]Department of Chemistry, University College London, 21 Gordon Street, WC1H 0AJ, London, UK

[b]UK Catalysis Hub, Rutherford Appleton Laboratory, Research Complex at Harwell, Harwell, Didcot, OX11 0FA, UK

[c]Finden Ltd. Clifton Hampden, Oxfordshire, OX14 3EE, UK

[d]Dinex Ecocat Oy, DET Finland, Catalyst development, Typpitie 1, FI-90620 Oulu, Finland.

*Author to whom correspondence should be addressed: Andrew.Beale@ucl.ac.uk

The ESI contains corresponding characterisation data for the VSCR1 catalysts.

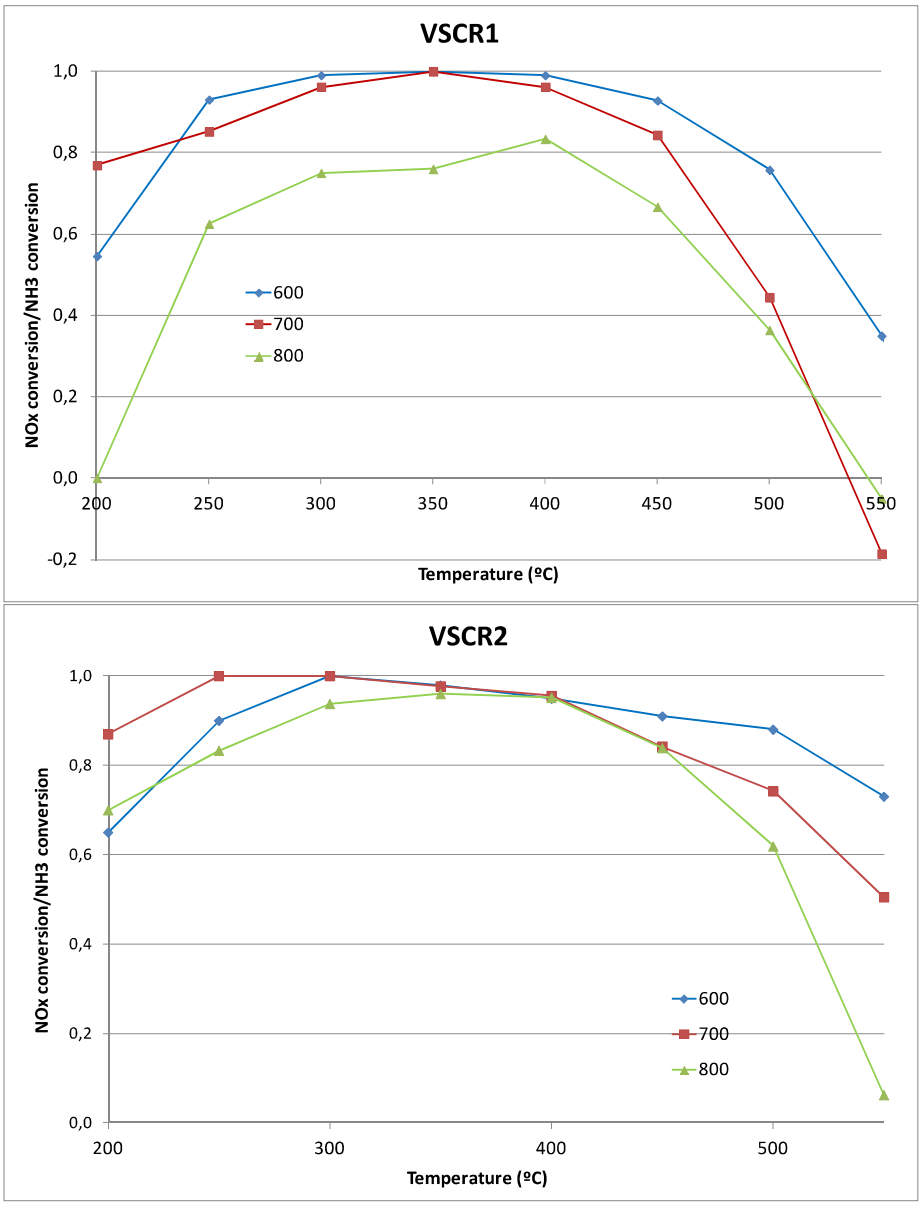

***ESI Figure 1**. Ratio between converted NO_x and converted NH_3 of both thermally aged VSCR1 (top) and VSCR2 (bottom) samples under Standard SCR conditions.*

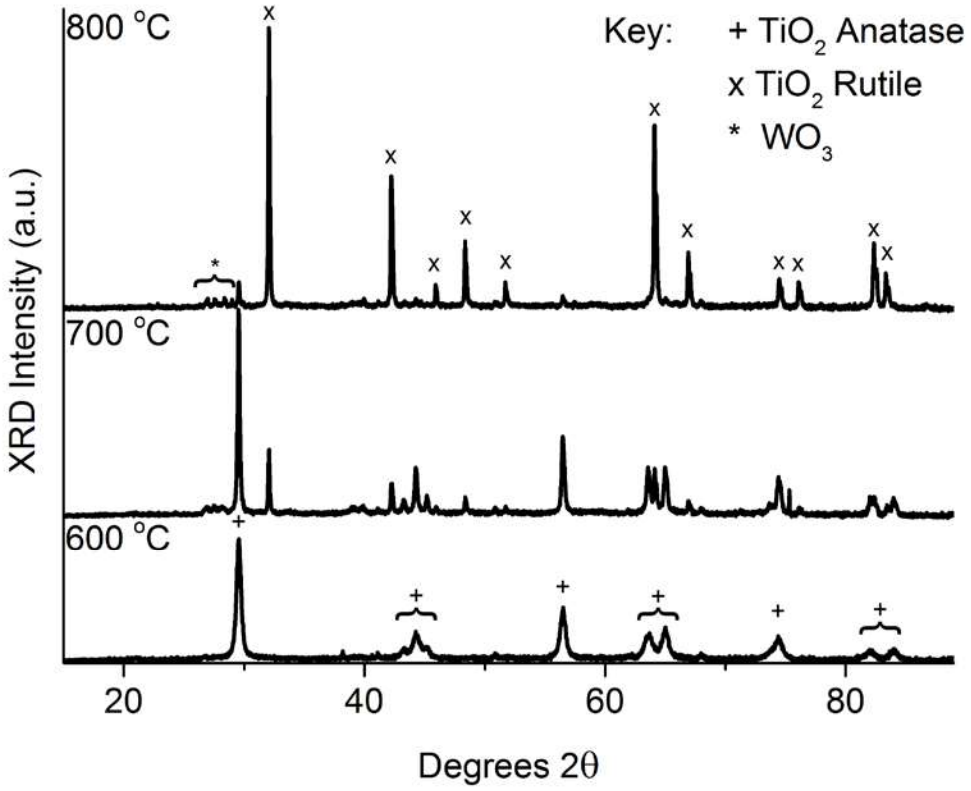

ESI Figure 2. *XRD data from the VSCR1 with increasing temperature of hydrothermal treatment. The important Bragg peaks for the respective phases TiO_2 Anatase, TiO_2 Rutile and monoclinic WO_3 have been identified with a **+**, **x** or ***** accordingly. Table 1 in the main text contains a list of the seven most pertinent reflections of each phase present.*

Table ESI 1. *First seven strong reflections from the main crystalline phases present (Co K_a source).*

Phase	Space group	Reflections present and position (° 2θ)	Lattice parameters
TiO_2 (Anatase)	I 41/a m d	(101) 29.51 (103) 43.18 (004) 44.18 (112) 45.10 (200) 56.42 (105) 63.49 (211) 64.93	a = b = 3.785 Å c = 9.514 Å
TiO_2 (Rutile)	P 42/m n m	(110) 31.97 (101) 42.15 (200) 45.84 (111) 48.27 (210) 51.62 (211) 64.02 (220) 66.83	a = b = 4.594 Å c = 2.959 Å
WO_3 (monoclinic)	P 121/c1	(200) 26.77 (020) 27.36 (002) 28.27 (022) 38.65 (202) 39.15 (202) 39.50 (220) 39.75	c = 9.511 Å

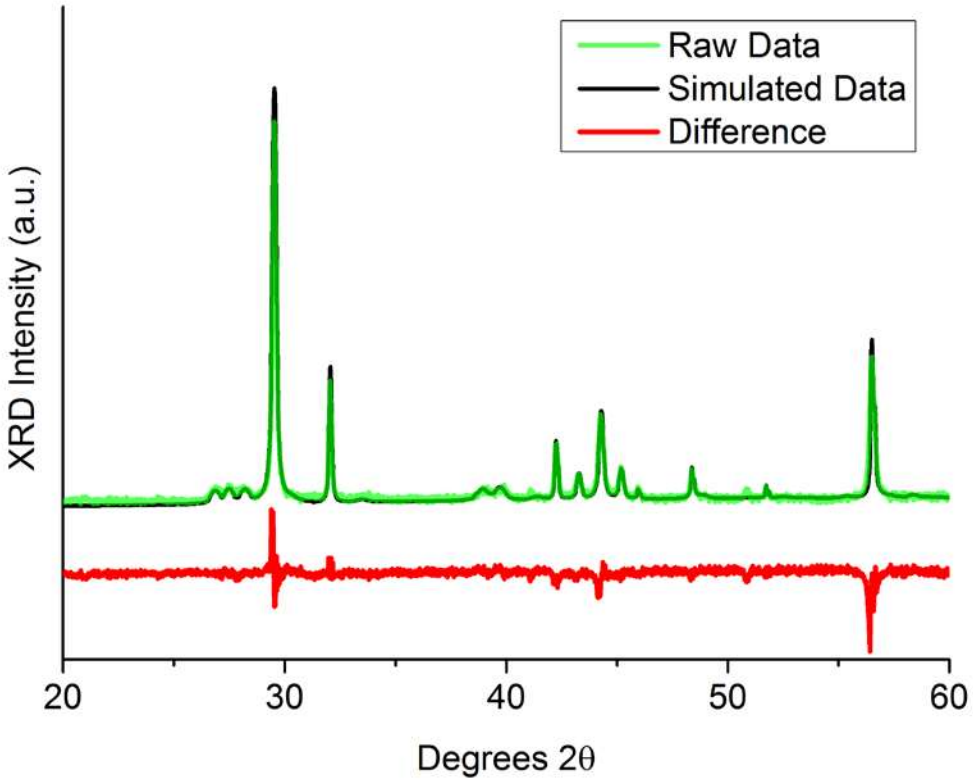

ESI Figure 3. *Experimental XRD pattern (black line), Rietveld-refined profile (light green line), and fitting residual (red line) for the VSCR2-800 °C sample. The phase composition extracted from the analysis is given in Table 1 in the main paper.*

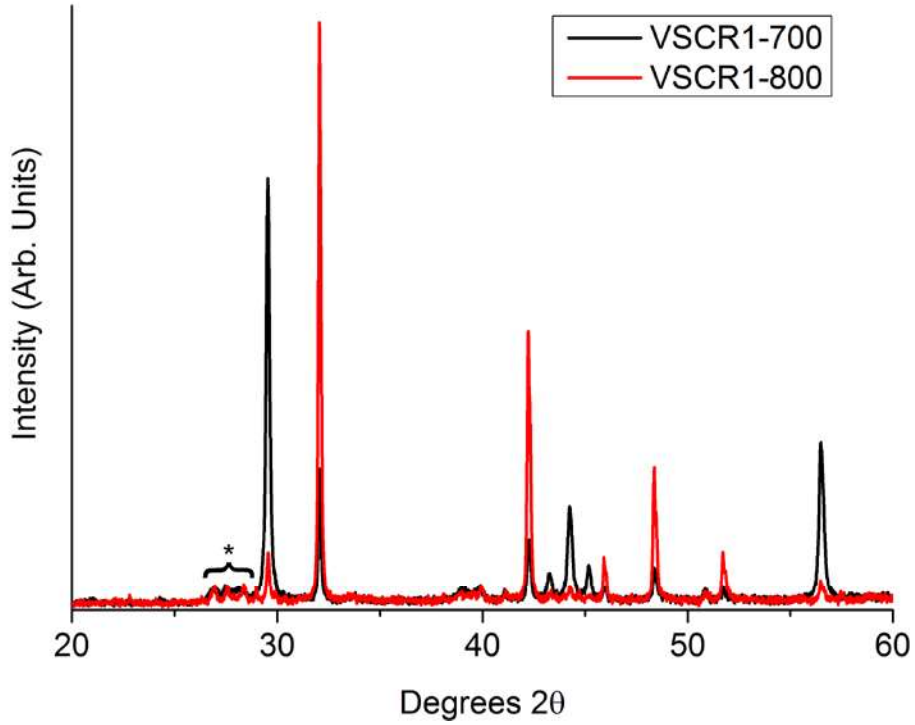

ESI Figure 4. *Comparative XRD patterns for the VSCR1-700 and VSCR1-800 samples illustrating the comparable XRD intensity of the monoclinic WO_3 phase (asterisked).*

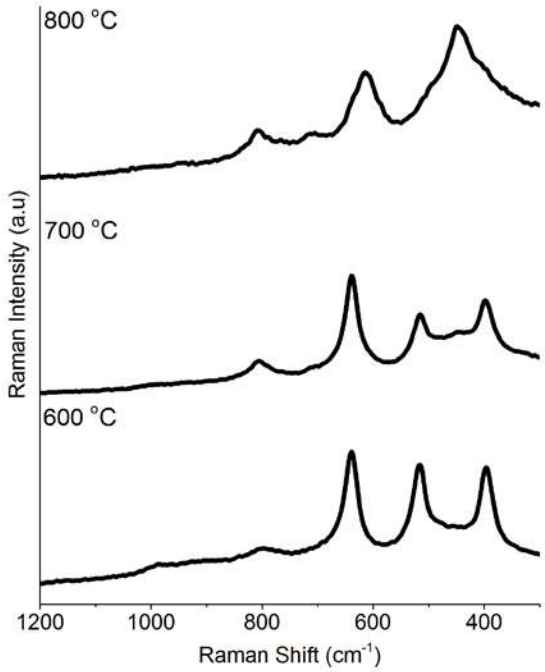

ESI Figure 5. *Raman data from the VSCR1 with increasing temperature of hydrothermal treatment. The band assignments and results from the peak profiling are given in Table 2 (main text).*

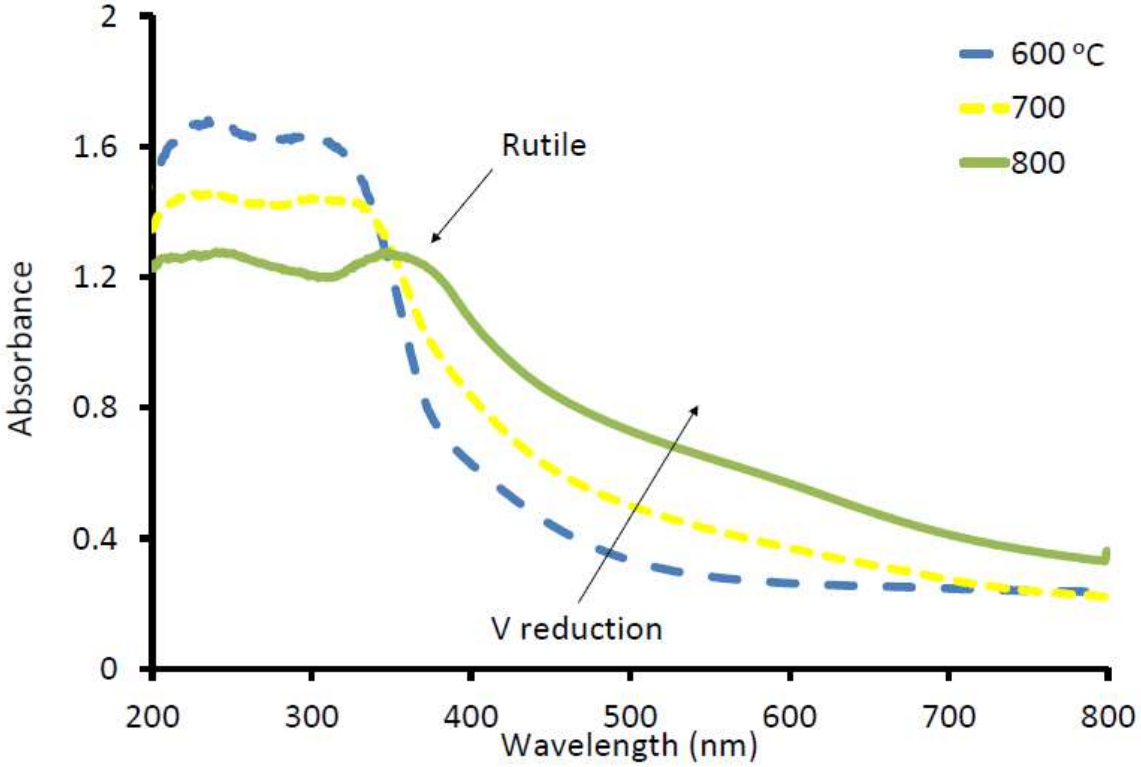

ESI Figure 6. *UV-Vis spectra for the VSCR1 with increasing temperature of hydrothermal treatment. The arrows indicate the shifts in either the LMCT band position (due to TiO_2 Rutile formation) or else the increased absorption in the visible region due to reduction of V species. The LMCT bands present in the spectra are listed in Table 3.*

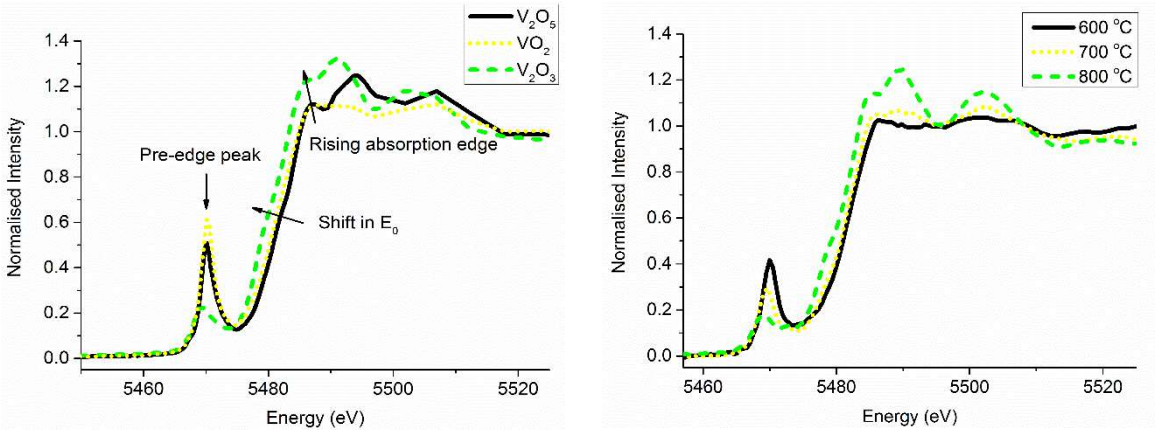

ESI Figure 7. *XANES spectra for the various vanadium oxide reference samples (left) and the VSCR1 after hydrothermal treatment at three different temperatures. The key features including the pre-edge peak, E_0 position and the rising absorption edge and their tendency with increasing treatment temperature have been highlighted using arrows.*

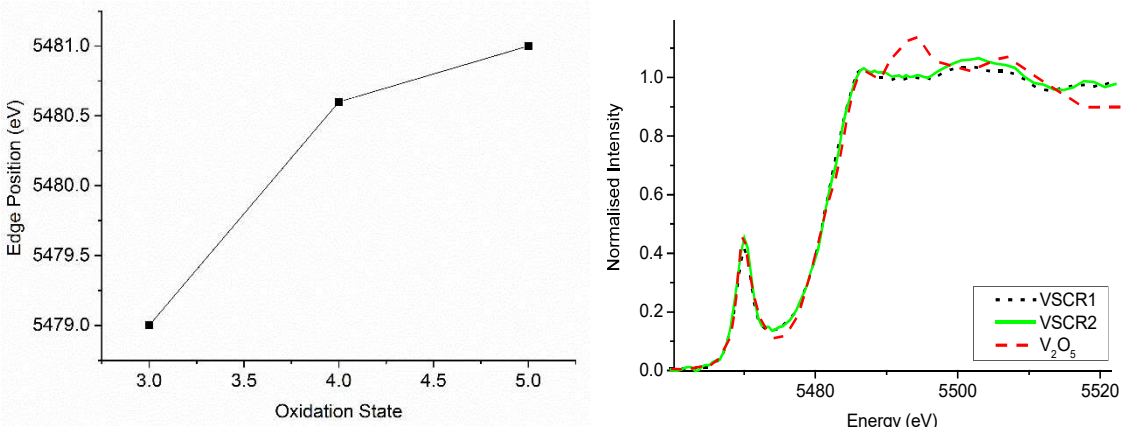

ESI Figure 8. *(Left) Plot of edge position (50 % of the normalised rising absorption edge intensity) vs. oxidation state from the reference compounds V_2O_3, VO_2 and V_2O_5. (Right) Normalised V K-edge XANES plot comparing the similarity of the pre-edge peak of VSCR1 and VSCR2 with crystalline V_2O_5.*

Table ESI 3. *XPS data for VSCR1 and VSCR2. Table shows surface composition in atomic%. The Vanadium $2p_{3/2}$ peak was asymmetric in all samples and was fitted with two components with binding energies 517.5 eV and 516.5 eV. These correspond to V^{5+} and V^{4+} respectively*

Sample	$V2p_{3/2}$ 517.5 eV (V^{5+})	$V2p_{3/2}$ 516.5 eV (V^{4+})	W4f	Ti2p	V^{5+} / (V^{5+}+V^{4+})
VSCR1-600	3.3	2.6	16.4	77.8	0.56
VSCR1-700	8.7	3.4	14.5	73.3	0.72
VSCR1-800	4.3	2.9	22.0	70.1	0.59
VSCR2-600	2.4	2.2	15.2	80.2	0.52
VSCR2-700	3.4	2.4	16.3	77.9	0.59
VSCR2-800	5.9	3.1	16.1	74.3	0.66